Joint simultaneous inversion of PP and PS angle gathers

Brian H. Russell, Daniel P. Hampson, Keith Hirsche, and Janusz Peron

ABSTRACT

We present a new approach to the joint simultaneous inversion of *PP* and *PS* angle gathers for the estimation of P-impedance, S-impedance and density. Our algorithm is based on three assumptions. The first is that the linearized approximation for reflectivity holds. The second is that *PP* and *PS* reflectivity as a function of angle can be given by the Aki-Richards linearized equations (Aki and Richards, 2002). The third is that there is a linear relationship between the logarithm of P-impedance and both S-impedance and density. Given these three assumptions, we show how a final estimate of P-impedance, S-impedance and density can be found by perturbing an initial P-impedance model. After a description of the algorithm, we then apply our method to both model and real data sets.

INTRODUCTION

The goal of pre-stack seismic inversion is to obtain reliable estimates of P-wave velocity (V_P), S-wave velocity (V_S), and density (ρ) from which to predict the fluid and lithology properties of the subsurface of the earth. This problem has been discussed by several authors. Simmons and Backus (1996) invert for linearized P-reflectivity (R_P), S-reflectivity (R_S) and density reflectivity (R_D), where

$$R_P = \frac{1}{2}\left[\frac{\Delta V_P}{V_P} + \frac{\Delta \rho}{\rho}\right], \tag{1}$$

$$R_S = \frac{1}{2}\left[\frac{\Delta V_S}{V_S} + \frac{\Delta \rho}{\rho}\right], \tag{2}$$

and

$$R_D = \frac{\Delta \rho}{\rho}\ . \tag{3}$$

Simmons and Backus (1996) also make three other assumptions: that the reflectivity terms given in equations (1) through (3) can be estimated from the angle dependent reflectivity $R_{PP}(\theta)$ by the Aki-Richards linearized approximation (Aki and Richards, 2002, Richards and Frasier, 1976), that ρ and V_P are related by Gardner's relationship (Gardner et al. 1974), given by

$$\frac{\Delta \rho}{\rho} = \frac{1}{4}\frac{\Delta V_P}{V_P}\ , \tag{4}$$

and that V_S and V_P are related by Castagna's equation (Castagna et al., 1985), given by

$$V_S = (V_P - 1360)/1.16. \tag{5}$$

The authors then use a linearized inversion approach to solve for the reflectivity terms given in equations (1) through (3).

Buland and Omre (2003) use a similar approach which they call Bayesian linearized AVO inversion. Unlike Simmons and Backus (1996), their method is parameterized by the three terms $\Delta V_P / V_P$, $\Delta V_S / V_S$, and $\Delta\rho / \rho$, again using the Aki-Richards approximation. The authors also use the small reflectivity approximation to relate these parameter changes to the original parameter itself. That is, for changes in P-wave velocity they write

$$\frac{\Delta V_P}{V_P} \approx \Delta \ln V_P . \tag{6}$$

where ln represents the natural logarithm. Similar terms are given for changes in both S-wave velocity and density. This logarithmic approximation allows Buland and Omre (2003) to invert for velocity and density, rather than reflectivity, as in the case of Simmons and Backus (1996).

In the present study, we present a new approach that allows us to invert directly for P-impedance ($Z_P=\rho V_P$), S-impedance ($Z_S=\rho V_S$), and density through a small reflectivity approximation similar to that of Buland and Omre (2003), and using constraints similar to those used by Simmons and Backus (1996). It is also our goal to extend an earlier post-stack impedance inversion method (Russell and Hampson, 1991) so that this method can be seen as a generalization to pre-stack inversion. The input data used to extract impedance and density consists of *PP* and, optionally, *PS* angle gathers, so we refer to the method as joint simultaneous inversion.

THEORY

We start by reviewing the principles of model-based post-stack inversion (Russell and Hampson, 1991). First, by combining equations (1) and (6), we can show that the small reflectivity approximation for the P-wave reflectivity is given by

$$R_{Pi} \approx \frac{1}{2}\Delta \ln Z_{Pi} = \frac{1}{2}\left[\ln Z_{Pi+1} - \ln Z_{Pi}\right], \tag{7}$$

where i represents the interface between layers i and $i+1$. If we consider an N sample reflectivity, equation (7) can be written in matrix form as

$$\begin{bmatrix} R_{P1} \\ R_{P2} \\ \vdots \\ R_{PN} \end{bmatrix} = \frac{1}{2}\begin{bmatrix} -1 & 1 & 0 & \cdots \\ 0 & -1 & 1 & \ddots \\ 0 & 0 & -1 & \ddots \\ \vdots & \ddots & \ddots & \ddots \end{bmatrix}\begin{bmatrix} L_{P1} \\ L_{P2} \\ \vdots \\ L_{PN} \end{bmatrix}, \tag{8}$$

where $L_{Pi} = \ln(Z_{Pi})$.

Next, if we represent the seismic trace as the convolution of the seismic wavelet with the earth's reflectivity, we can write the result in matrix form as

$$\begin{bmatrix} T_1 \\ T_2 \\ \vdots \\ T_N \end{bmatrix} = \begin{bmatrix} w_1 & 0 & 0 & \cdots \\ w_2 & w_1 & 0 & \ddots \\ w_3 & w_2 & w_1 & \ddots \\ \vdots & \ddots & \ddots & \ddots \end{bmatrix} \begin{bmatrix} R_{P1} \\ R_{P2} \\ \vdots \\ R_{PN} \end{bmatrix}, \tag{9}$$

where T_i represents the i^{th} sample of the seismic trace and w_j represents the j^{th} term of an extracted seismic wavelet. Combining equations (8) and (9) gives us the forward model which relates the seismic trace to the logarithm of P-impedance:

$$T = (1/2)WDL_P \quad , \tag{10}$$

where W is the wavelet matrix given in equation (9) and D is the derivative matrix given in equation (8). If equation (10) is inverted using a standard matrix inversion technique to give an estmate of L_P from a knowledge of T and W, there are two problems. First, the matrix inversion is both costly and potentially unstable. More importantly, a matrix inversion will not recover the low frequency component of the impedance. An alternate strategy, and the one adopted in our implementation of equation (10), is to build an initial guess impedance model and then iterate towards a solution using the conjugate gradient method.

We can now extend the theory to the pre-stack inversion case. The Aki-Richards equation was re-expressed by Fatti et al. (1994) as

$$R_{PP}(\theta) = c_1 R_P + c_2 R_S + c_3 R_D \quad , \tag{11}$$

where $c_1 = 1 + \tan^2\theta$, $c_2 = -8\gamma^2 \tan^2\theta$, $\gamma = V_S / V_P$, $c_3 = -0.5\tan^2\theta + 2\gamma^2 \sin^2\theta$, and the three reflectivity terms are as given by equations (1) through (3).

For a given angle trace $T(\theta)$ we can therefore extend the zero offset (or angle) trace given in equation (10) by combining it with equation (11) to get

$$T(\theta) = (1/2)c_1 W(\theta)DL_P + (1/2)c_2 W(\theta)DL_S + W(\theta)c_3 DL_D \quad , \tag{12}$$

where $L_S = \ln(Z_S)$ and $L_D = \ln(\rho)$. Note that the wavelet is now dependent on angle. Equation (12) could be used for inversion, except that it ignores the fact that there is a relationship between L_P and L_S and between L_P and L_D. Because we are dealing with impedance rather than velocity, and have taken logarithms, our relationships are different than those given by Simmons and Backus (1996) and are given by

$$\ln(Z_S) = k \ln(Z_P) + k_c + \Delta L_S \quad , \tag{13}$$

and

$$\ln(Z_D) = m\ln(Z_P) + m_c + \Delta L_D \quad . \tag{14}$$

That is, we are looking for deviations away from a linear fit in logarithmic space. This is illustrated in Figure 1.

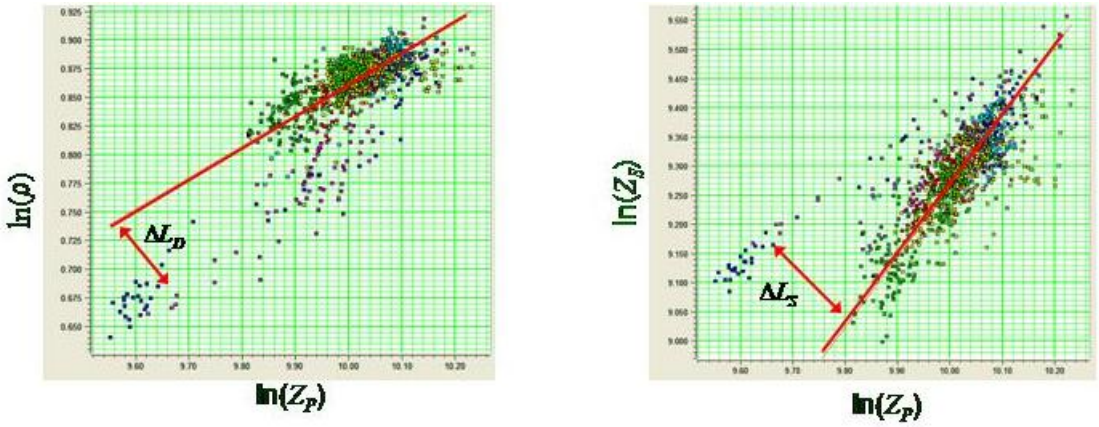

(a) *(b)*

FIG. 1. Crossplots of (a) $\ln(Z_D)$ vs $\ln(Z_P)$ and (b) $\ln(Z_S)$ vs $\ln(Z_P)$ where, in both cases, a best straight line fit has been added. The deviations away from this straight line, ΔL_D and ΔL_S, are the desired fluid anomalies.

Combining equations (12) through (14), we get

$$T(\theta) = \tilde{c}_1 W(\theta) D L_P + \tilde{c}_2 W(\theta) D \Delta L_S + W(\theta) c_3 D \Delta L_D \quad , \tag{15}$$

where $\tilde{c}_1 = (1/2)c_1 + (1/2)kc_2 + mc_3$ and $\tilde{c}_2 = (1/2)c_2$. Equation (15) can be implemented in matrix form as

$$\begin{bmatrix} T(\theta_1) \\ T(\theta_2) \\ \vdots \\ T(\theta_N) \end{bmatrix} = \begin{bmatrix} \tilde{c}_1 W(\theta_1) D & \tilde{c}_2 W(\theta_1) D & c_3 W(\theta_1) D \\ \tilde{c}_1 W(\theta_2) D & \tilde{c}_2 W(\theta_2) D & c_3 W(\theta_2) D \\ \vdots & \vdots & \vdots \\ \tilde{c}_1 W(\theta_N) D & \tilde{c}_2 W(\theta_N) D & c_3 W(\theta_N) D \end{bmatrix} \begin{bmatrix} L_P \\ \Delta L_S \\ \Delta L_D \end{bmatrix}, \tag{16}$$

If equation (16) is solved by matrix inversion methods, we again run into the problem that the low frequency content cannot be resolved. A practical approach is to initialize the solution to $\begin{bmatrix} L_P & \Delta L_S & \Delta L_D \end{bmatrix}^T = \begin{bmatrix} \ln(Z_{P0}) & 0 & 0 \end{bmatrix}^T$, where ZP0 is the initial impedance model, and then to iterate towards a solution using the conjugate gradient method.

We will now extend the previous derivation to include pre-stack converted-wave measurements (*PS* gathers) that have been converted to *PP* time. We will use the linearized form of the equation was developed by Aki, Richards, and Frasier (Aki and Richards, 2002, Richards and Frasier, 1976). It has been shown by Margrave et al. (2001) that this equation can be written as

$$R_{PS}(\theta,\phi) = c_4 R_S + c_5 R_D \quad , \tag{17}$$

where $c_4 = \frac{\tan\phi}{\gamma}\left[4\sin^2\phi - 4\gamma\cos\theta\cos\phi\right]$, $c_5 = \frac{-\tan\phi}{2\gamma}\left[1 + 2\sin^2\phi - 2\gamma\cos\theta\cos\phi\right]$, $\gamma = V_S / V_P$, and $\phi = \sin^{-1}(\gamma\sin\theta)$. The reflectivity terms R_S and R_D given in equation (17) are identical to the terms those given in equations (2) and (3). Using the small reflectivity approximation, we can therefore re-write equation (17) as:

$$T_{PS}(\theta,\phi) = c_4 W(\phi) DL_S + c_5 W(\phi) DL_D \quad . \tag{18}$$

Next, using the relationships between S-impedance, density and P-impedance given in equations (13) and (14), equation (18) can be further re-written as

$$T_{PS}(\theta,\phi) = \tilde{c}_4 W(\phi) DL_P + c_4 W(\phi) D\Delta L_S + c_5 W(\phi) D\Delta L_D , \tag{19}$$

where $\tilde{c}_4 = kc_4 + mc_5$.

Note that equation (19) allows us to express a single *PS* angle stack as a function of the same three parameters given in equation (15). Also, equation (19) is given at a single angle ϕ. When we generalize this equation to *M* angle stacks, we can combine this relationship with equation (16) and write the general matrix equation as

$$\begin{bmatrix} T_{PP}(\theta_1) \\ \vdots \\ T_{PP}(\theta_N) \\ T_{PS}(\phi_1) \\ \vdots \\ T_{PS}(\phi_M) \end{bmatrix} = \begin{bmatrix} \tilde{c}_1(\theta_1)W(\theta_1)D & c_2(\theta_1)W(\theta_1)D & c_3(\theta_1)W(\theta_1)D \\ \vdots & \vdots & \vdots \\ \tilde{c}_1(\theta_N)W(\theta_N)D & c_2(\theta_N)W(\theta_N)D & c_3(\theta_N)W(\theta_N)D \\ \tilde{c}_4(\phi_1)W(\phi_1)D & c_4(\phi_1)W(\phi_1)D & c_5(\phi_1)W(\phi_1)D \\ \vdots & \vdots & \vdots \\ \tilde{c}_4(\phi_M)W(\phi_M)D & c_4(\phi_M)W(\phi_M)D & c_5(\phi_M)W(\phi_M)D \end{bmatrix} \begin{bmatrix} L_P \\ \Delta L_S \\ \Delta L_D \end{bmatrix} . \tag{20}$$

Equation (20) gives us a general expression for the simultaneous inversion of *N PP* angle stacks and *M PS* angle stacks. Note that we extract a different wavelet for each of the *PS* angle stacks, as was done for each of the *PP* angle stacks.

MODEL EXAMPLE

We will now apply this method to a model data example. To create this model, we started with a measured set of well logs (P-wave, S-wave, density, and computed Poisson's ratio) for a well in which the in-situ case was a partially saturated gas sand. We then used the Biot-Gassmann equations to perform fluid substitution and create a number of model scenarios ranging from the 100% wet case to the 100% gas case, in increments of 10% saturation (except between S_W values of 90% and 100%, where we inserted the 95% case). We created the equivalent well log curves for each case, as well as a model synthetic, using a wave equation modeling algorithm with a 40 hertz Ricker wavelet. The model synthetic was then used as the input data for a series of inversions at

each value of S_W. A detailed analysis of the two end members (the gas case and wet case) is shown in Figures 2 and 3.

Figure 2(a) shows the well log curves for a gas sand on the left (in blue), with the initial guess curves (in red) set to be extremely smooth so as not to bias the solution. On the right we show the model synthetic angle gather computed from the inversion algorithm, the input computed angle gather from the full well log curves, and the error, which is almost identical to the input. The far angle trace for the model and input angle synthetics is 60^o.

Figure 2(b) then shows the same displays after 20 iterations through the conjugate gradient inversion process. Note that the final estimates of the well log curves match the initial curves quite well for the P-impedance, Z_P, S-impedance, Z_S, and the Poisson's ratio (σ). The density (ρ) shows some "overshoot" above the gas sand (at 3450 ms), but agrees with the correct result within the gas sand. The results on the right of Figure 2(b) show that the error is now very small.

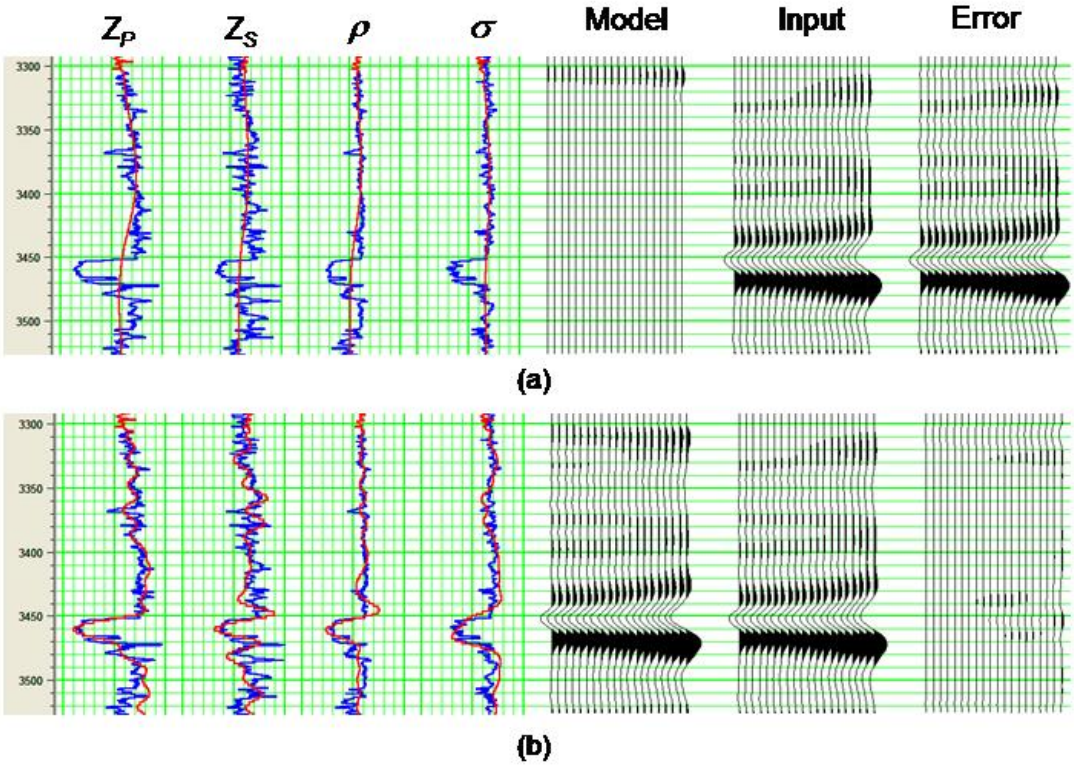

FIG. 2. The results of inverting a gas sand model, where (a) shows the initial model before inversion, and (b) shows the results after inversion.

The equivalent wet model for the gas sand shown in Figure 2 is shown in Figure 3. We again performed inversion on this model dataset. Figure 3(a) shows the well log curves for the wet sand on the left, with the smooth initial guess curves superimposed in red. On the right we show the model synthetic angle gather computed from the inversion algorithm, the input computed angle gather from the full well log curves, and the error,

which is almost identical to the input. The far angle trace for the model and input angle synthetics is again 60°.

Figure 3(b) then shows the same displays after 20 iterations through the conjugate gradient inversion process. As in the gas case, the final estimates of the well log curves match the initial curves quite well, especially for the P-impedance, Z_P, S-impedance, Z_S, and the Poisson's ratio (σ). The density (ρ) shows a much better fit at the wet sand (which is at 3450 ms) than it did at the gas sand in Figure 2.

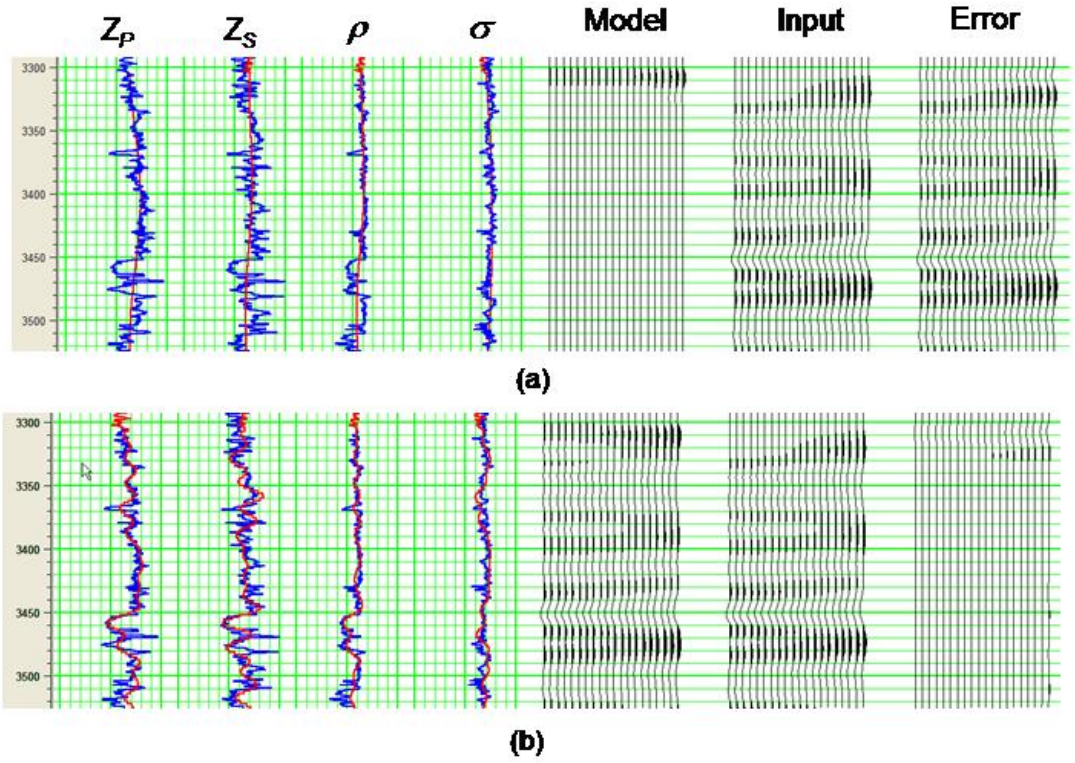

FIG. 3. The results of inverting a wet sand model, where (a) shows the initial model before inversion, and (b) shows the results after inversion.

The results shown in Figures 2 and 3 show us that the inversion algorithm is performing very well. However, it should be pointed out that this is noise-free data with an angular aperture of 60 degrees, which is very optimistic when compared with real data apertures.

Finally, Figure 4 shows the inverted results at each of the twelve different values of water saturation. Figure 4(a) shows the P-impedance values in colour, with the colour scale on the left. Figure 4(b) shows the V_P/V_S ratio results in colour, with the colour scale again on the left. In both Figures, the seismic inversion results at the wells have been duplicated five times for clarity, but the original P-wave velocity log has been shown only once.

In Figure 4, notice that both the P-impedance and V_P/V_S ratio results are consistent with the fact that the gas sand is changing to a wet sand as we move from left to right along the plots.

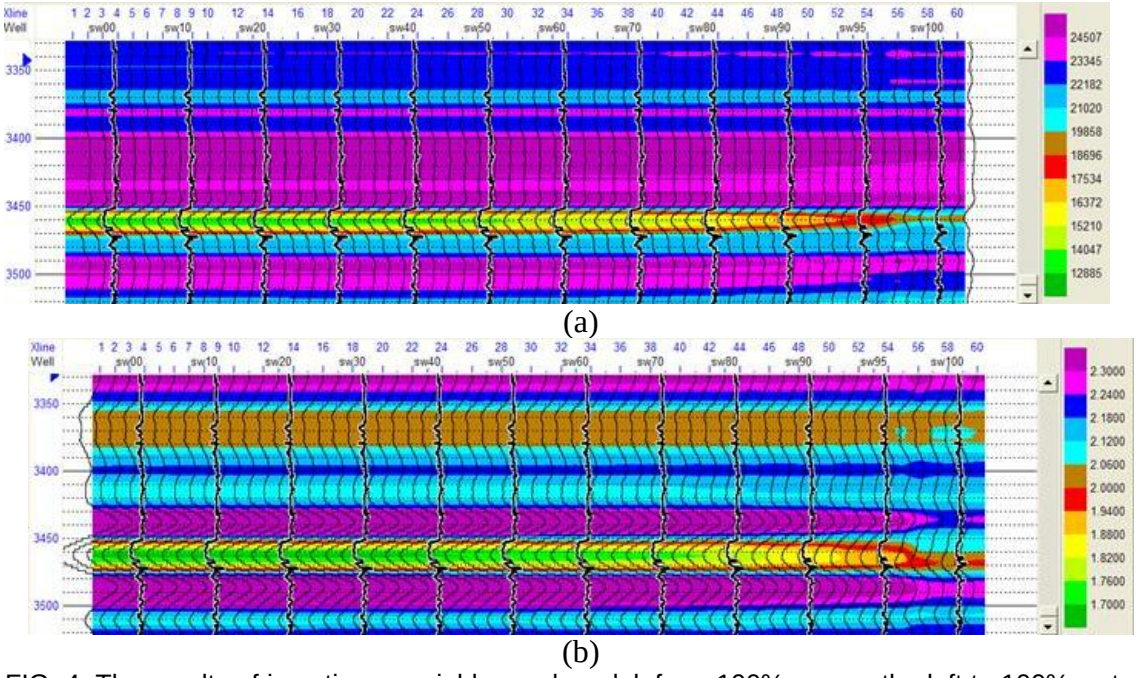

FIG. 4. The results of inverting a variable sand model, from 100% gas on the left to 100% wet on the right where (a) shows the P-impedance results, and (b) shows the V_P/V_S ratio results.

PP DATA EXAMPLE

We will next look at a real data example, consisting of a shallow Cretaceous gas sand from central Alberta. Figure 5 shows the computed V_P/V_S ratio from this dataset, where the anomalous gas sand is encircled by the black ellipse. Notice the drop in V_P/V_S associated with the gas sand.

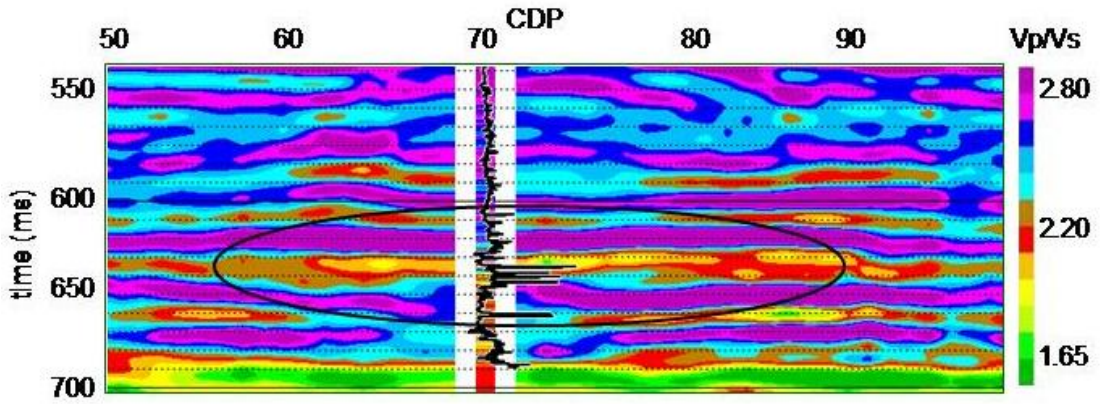

FIG. 5. The inverted V_P/V_S ratio for a shallow gas sand from Alberta, where the ellipse indicates the anomalous region.

Figure 6 then shows a comparison between the input gathers over the sand (where a clear AVO Class 3 anomaly is evident), and the computed synthetic gathers using the inverted results.

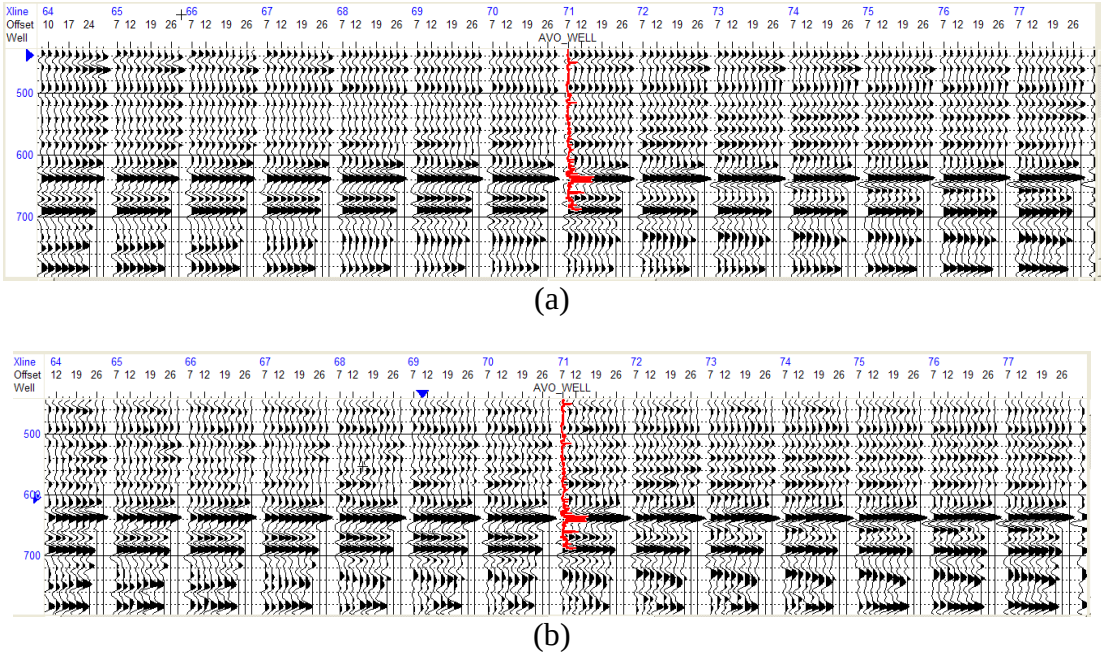

FIG. 6. The CDP gathers over the gas sand anomaly from Fig.4, where (a) shows the input gathers and (b) shows the synthetic gathers after inversion.

Note that the results given in Figure 6 show that a very good fit to the original real data can be obtained by applying forward modeling to the well logs obtained from the inversion process. This can be considered as an excellent diagnostic, but is not to be interpreted as indicating that our result is absolutely correct, since there is possible non-uniqueness in the answer.

PP-PS DATA EXAMPLE

In this final example, we will show a joint PP-PS inversion using a case study from northeastern Alberta. The workflow for this example involved the following steps:

1. Correlate the *PP* and *PS* data to wells
2. Pick the corresponding horizons on both datasets.
3. Use horizon based event matching to convert PS data to PP time.
4. Invert *PP* and *PS* data using simultaneous inversion.

Figure 7(a) shows the correlated *PP* data and Figure 7(b) shows the correlated PS data from our example, where the P-wave, S-wave, and density logs are shown on the left of each figure, and the stacked data (*PP* or *PS*) is shown on the right. The synthetic trace (blue) to seismic trace (red) correlation is shown between the logs and the stacked data.

Note that the ties are quite reasonable in both cases shown. The wavelets used to create the synthetic were extracted from the seismic data shown.

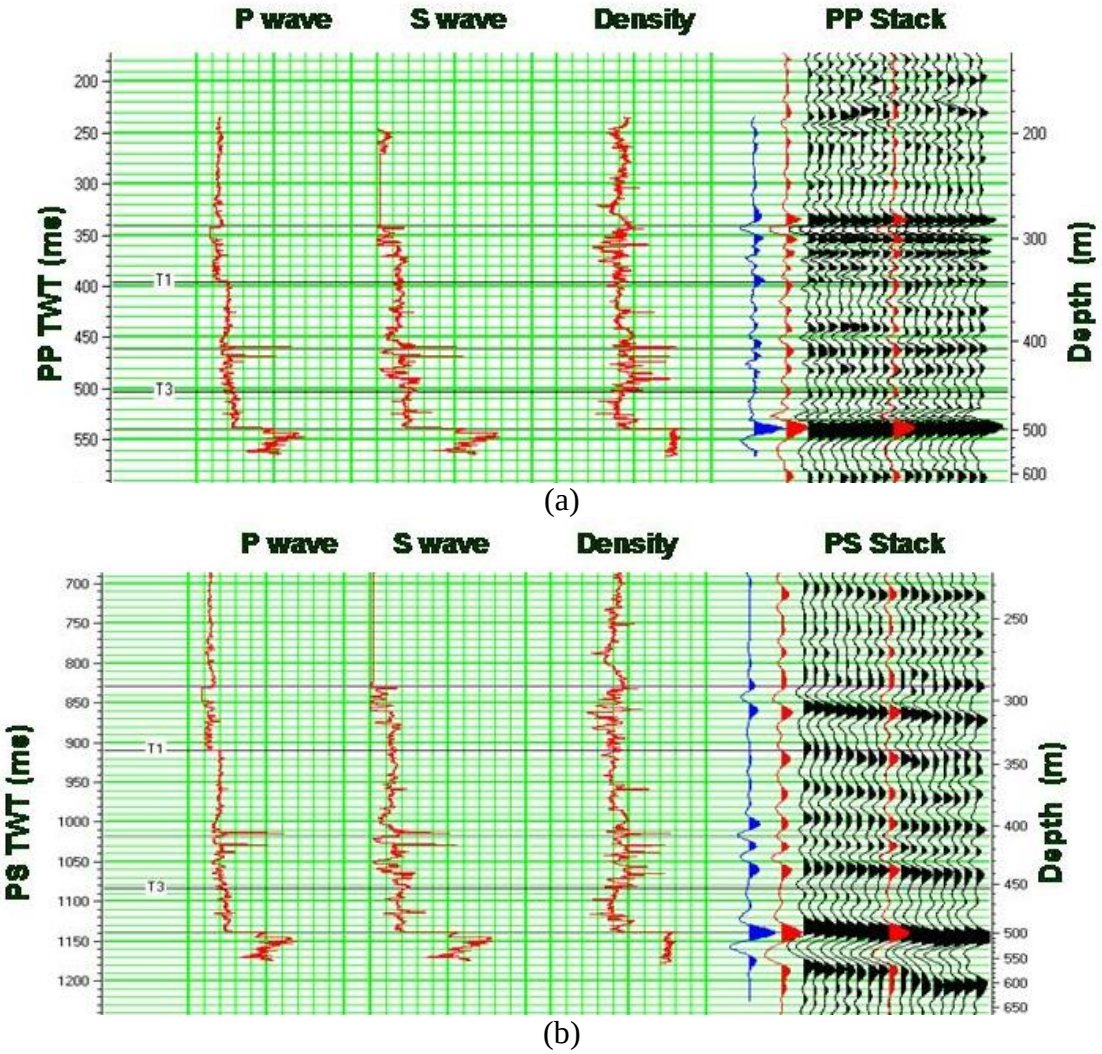

FIG. 7. The correlation results, where (a) shows the logs on the left and the PP stack on the right, and (b) shows the logs on the left and the PS stack on the right. The blue trace shows the synthetic and the red trace shows the extracted seismic.

We then performed two different types on inversion. The first type of inversion, which we will call independent inversion, involved building independent P and S-impedance models for the *PP* and *PS* stacks and using a model-based inversion algorithm to independently invert the two datasets. These models were created by interpolating well log values from eight wells which intersected the well log survey. This assumes that the *PP* stack is a good approximation to zero-offset *P*-reflectivity, and that the *PS* stack is a good approximation to zero-offset *S*-reflectivity.

The second inversion is referred to as joint inversion, and applies the theory discussed in earlier in this paper, specifically in equation 10. Notice that we have only two inputs: the *PP* stack and the *PS* stack. Thus, the problem is under-determined and we therefore decided not to invert for density, only for P and S-impedance. We assume that the *PP*

stack is equivalent to a *PP* angle gather at zero degrees and that the *PS* stack is equivalent to a *PS* angle stack at 20 degrees. The value of 20 degrees was arrived at by cross-correlating the traces in the PS stack with model traces at various angles.

To check the validity of the inversion, we performed cross-validation of the results at each of the eight wells which intersected the dataset. Cross-validation consists of leaving each well in turn out of the model-building process and then "blindly" predicting each well from the inversion results. This results of the cross-validation process are shown in Figure 8, where 8(a) shows the independent inversion results and 8(b) shows the joint inversion results for V_P/V_S ratio.

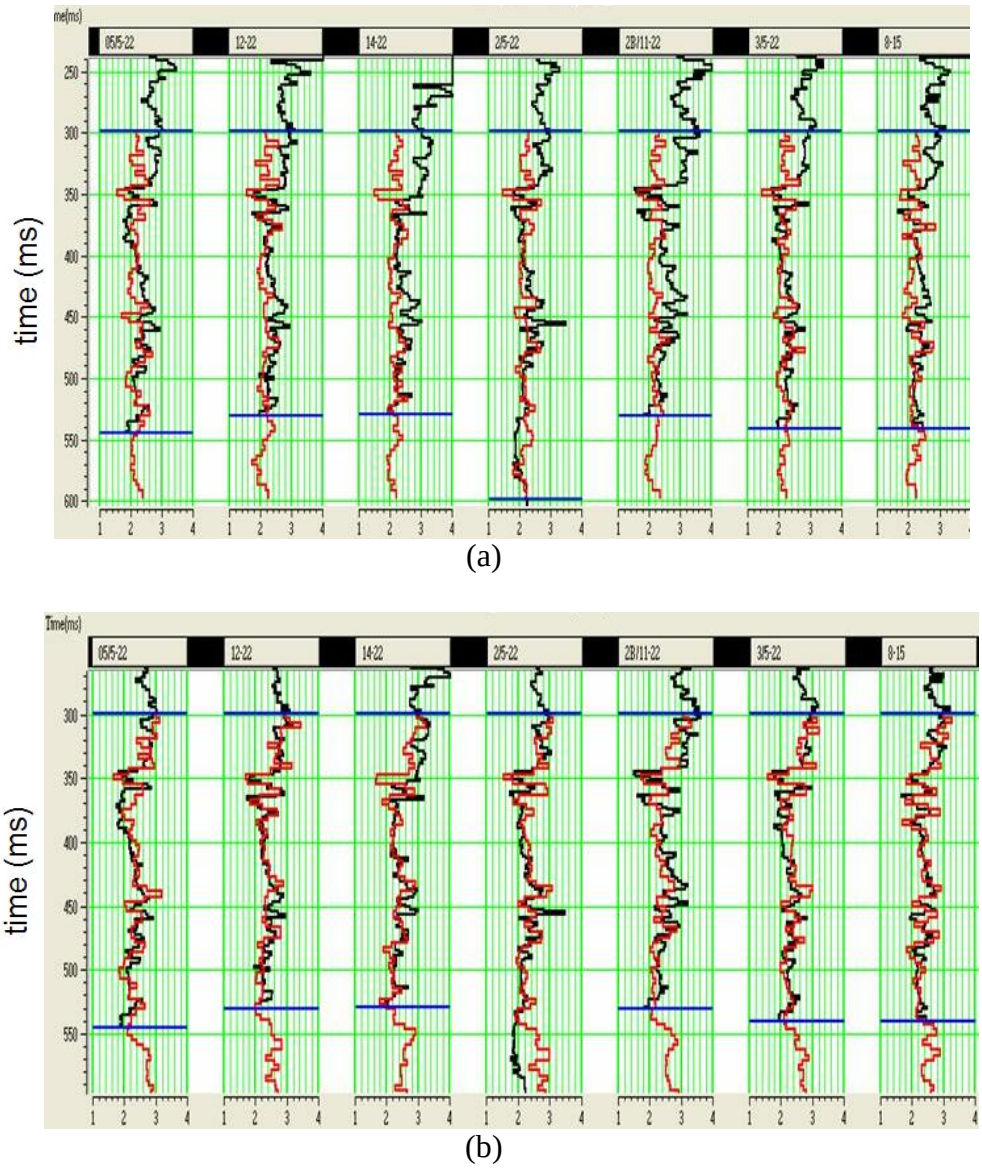

FIG. 8. The cross-validation of the inversion results at each of the well locations, where (a) shows the results of independent inversion, and (b) shows the results of joint inversion. The parameter being plotting is Vp/Vs ratio.

It is clear from Figure 8 that the joint inversion has created a better visual fit at the wells than independent inversion. To quantify this observation, Figure 9 shows the cross-correlation values at the wells, where Figure 9(a) corresponds to the independent inversion of Figure 8(a) and Figure 9(b) corresponds to the joint inversion of Figure 8(b). Notice that for the independent inversion (Figure 9(a)), the correlation coefficients are centered on a value of 0.25, whereas for the joint inversion (Figure 9(b)) the correlation coefficients are closer to a value of 0.75. It can be seen that only two of the wells drop below a 0.5 correlation for joint inversion, and these are the same two wells with a correlation close to zero on the independent inversion. This validates our qualitative observation from Figure 8, that the joint inversion has done a better job than the independent inversion.

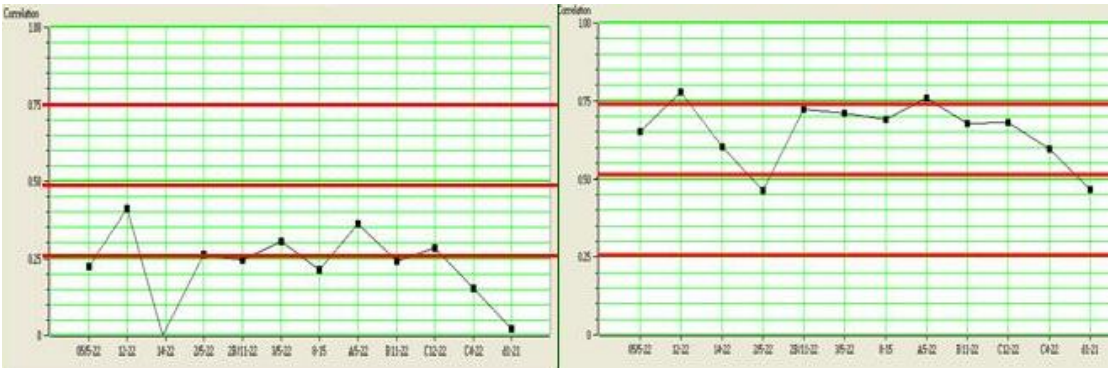

(a) (b)

FIG. 9. A display of the cross-correlation between the known Vp/Vs ratios from the wells and the inverted results of (a) Figure 8(a), the independent inversion, and (b) Figure 8(b), the joint inversion.

Finally, the results of applying the two inversion algorithms to the seismic datasets are shown in Figure 10, where the results have been shown for the V_P/V_S ratio. Figure 10(a) shows the result of independent inversion and Figure 10(b) shows the result of joint inversion. Note that the V_P/V_S ratio in colour on the inserted well log matches the colour on the inversion results and that the scale in shown on the right hand sides of the plots.

On the independent inversion results of Figure 10(a), note that the match between the well values and the seismic result is not very good, especially at the top of the section, between 300 and 350 ms, and the middle part of the section between 420 and 470 ms. The mismatch at the base of the section is due to the fact that the well log data has not been recorded below about 530 ms. On the joint inversion results of Figure 10(b) there is good agreement in the two zones just described, suggesting that the inversion has done a better job of matching the well results.

Based on the results seen in Figures 8 through 10, it seems clear that the joint inversion algorithm, in which the *PP* and *PS* data are coupled in the algorithm, is superior to the independent inversion, in which there is no coupling between the two datasets.

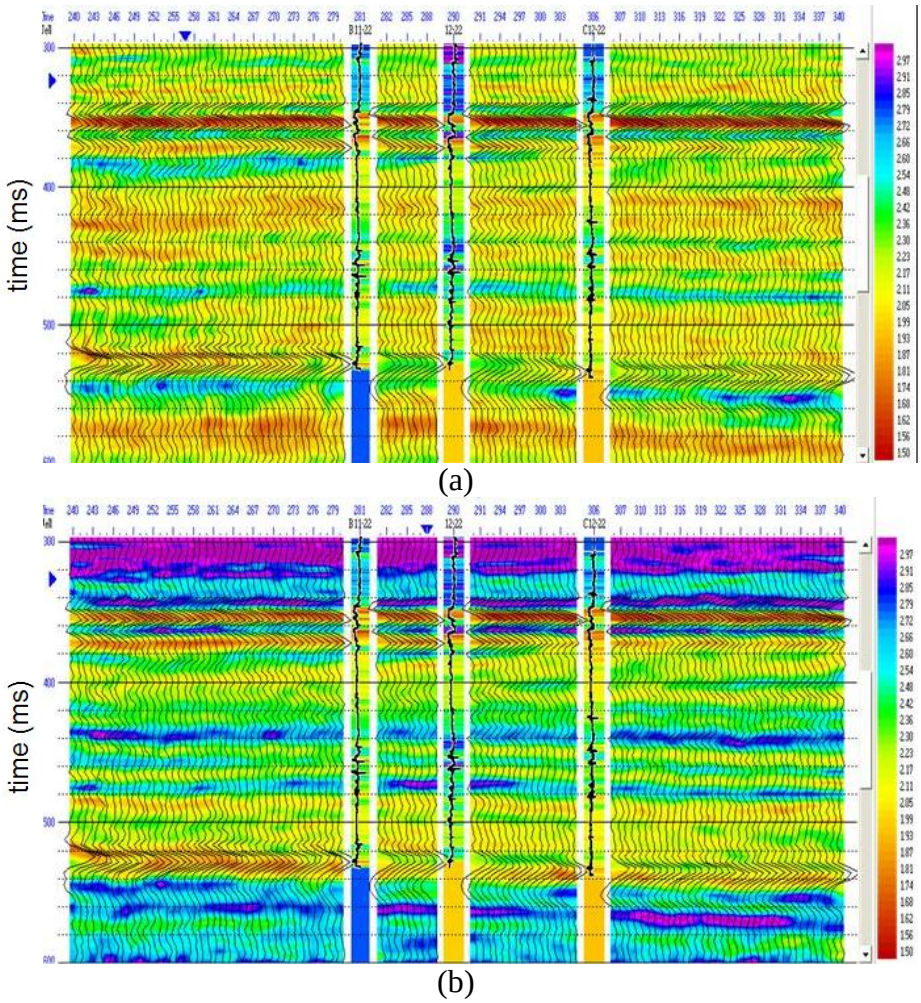

FIG. 10. The final inverted results for Vp/Vs ratio extracted from the seismic data using (a) independent inversion and (b) joint inversion.

CONCLUSIONS

We have presented a new approach to the joint simultaneous inversion of pre-stack seismic data which produces estimates of P-impedance, S-Impedance and density. This method allows us to incorporate both PP and PS data into the solution, if we have first calibrated both datasets to PP time. The method is based on three assumptions: that the linearized approximation for reflectivity holds, that reflectivity as a function of angle can be given by the Aki-Richards equations, and that there is a linear relationship between the logarithm of P-impedance and both S-impedance and density. Our approach was shown to work well for modelled gas and wet sands, for a real PP seismic example which consisted of a shallow Creataceous gas sand from Alberta, and for a joint PP-PS dataset from northeast Alberta. In the first two data examples, pre-stack PP seismic data was used. In the joint PP-PS dataset the prestack data was not available and we applied the method to full stacks. Future work will involve the incorporation of pre-stack PS data.

REFERENCES

Aki, K., and Richards, P.G., 2002, Quantitative Seismology, 2nd Edition: W.H. Freeman and Company.

Buland, A. and Omre, H, 2003, Bayesian linearized AVO inversion: Geophysics, **68**, 185-198.
Castagna, J.P., Batzle, M.L., and Eastwood, R.L., 1985, Relationships between compressional-wave and shear-wave velocities in clastic silicate rocks: Geophysics, **50**, 571-581.
Fatti, J., Smith, G., Vail, P., Strauss, P., and Levitt, P., 1994, Detection of gas in sandstone reservoirs using AVO analysis: a 3D Seismic Case History Using the Geostack Technique: Geophysics, **59**, 1362-1376.
Gardner, G.H.F., Gardner, L.W. and Gregory, A.R., 1974, Formation velocity and density - The diagnostic basics for stratigraphic traps: Geophysics, **50,** 2085-2095.
Margrave, G.F., Stewart, R. R. and Larsen, J. A., 2001, Joint *PP* and *PS* seismic inversion: The Leading Edge, **20,** no. 9, 1048-1052.
Richards, P. G. and Frasier, C. W., 1976, Scattering of elastic waves from depth-dependent inhomogeneities: Geophysics, **41,** 441-458.
Russell, B. and Hampson, D., 1991, A comparison of post-stack seismic inversion methods: Ann. Mtg. Abstracts, Society of Exploration Geophysicists, 876-878.
Simmons, J.L. and Backus, M.M., 1996, Waveform-based AVO inversion and AVO prediction-error: Geophysics, **61**, 1575-1588.

ACKNOWLEDGEMENTS

We wish to thank our colleagues at the CREWES Project and at Hampson-Russell Software for their support and ideas, as well as the sponsors of the CREWES Project.